fishes

MDPI

Article

Measurement and Numerical Modelling of Swim Bladder Resonance Properties of Recently Euthanised Brown Trout (*Salmo trutta*)

William Luocheng Wu [1,*], Philip Ericsson [2], Paul Kemp [2] and Paul Robert White [1]

[1] Institute of Sound and Vibration Research, University of Southampton, Southampton SO17 1BJ, UK; prw@soton.ac.uk
[2] International Centre for Ecohydraulics Research, University of Southampton, Southampton SO16 7QF, UK; p.ericsson@soton.ac.uk (P.E.); p.kemp@soton.ac.uk (P.K.)
* Correspondence: william.wu@soton.ac.uk

Abstract

Swim bladders in some teleost fish can act as gas-filled cavities that oscillate under acoustic pressure and transfer the sound energy to the inner ears. Quantifying the resonance frequency and damping of these oscillations is useful for linking swim bladder mechanics to hearing-related and behavioural questions, but many established direct-measure approaches have relied on open-water deployments and careful avoidance of boundary reflections, making experiments logistically demanding and difficult to reproduce (e.g., requiring deep-water sites, careful control of surface/boundary reflections, and complex deployment geometries). This study presents a compact laboratory methodology for estimating swim bladder resonance properties using a closed, fully water-filled, stainless-steel impedance tube. Broadband pseudorandom excitation is applied via an end-plate shaker, and the acoustic response of the system is recorded using wall-mounted hydrophones. Resonance peaks are identified using power spectral estimates of recorded signals, allowing resonance frequency and quality factor to be extracted from the peak location and −3 dB bandwidth. The approach is first established using inflated latex balloons as surrogate encapsulated gas cavities, providing a controlled benchmark for repeatability and interpretation. It is then applied to recently euthanised brown trout (*Salmo trutta*), where clear resonance features attributable to the swim bladder are observed and show systematic variation with body size. A coupled finite element model reproduces the principal resonance behaviour under the experimental loading and supports interpretation of the measured peaks as swim bladder resonance. The results provide a validated foundation for subsequent non-invasive measurements on live, free-swimming fish, as well as for future applications where swim bladder condition may be relevant to management or conservation.

Keywords: swim bladder; bubble resonance; underwater bioacoustics; finite element modelling

Key Contribution: This study demonstrates a compact, repeatable laboratory method for extracting swim bladder resonance frequency, as well as an operational quality factor in recently euthanised brown trout using a fully water-filled stainless-steel impedance tube and PSD-based peak analysis. Coupled finite element acoustic–structure simulations reproduce the observed resonance band under the experimental loading, providing mechanistic support for peak attribution and establishing a calibrated framework for subse-

Academic Editors: Xiaoqin Zang and Leif Rasmuson

Received: 31 January 2026
Revised: 5 March 2026
Accepted: 13 March 2026
Published: 15 March 2026

quent live-fish, non-invasive measurements and resonance-informed auditory/behavioural stimulus design.

1. Introduction

Aquatic environments contain a wide range of biologically, geophysically, and anthropogenically generated sounds, and many animals use acoustic cues to support behaviours such as habitat selection, predator avoidance, and social interactions [1–5]. For fishes, the relevant acoustic information includes both sound pressure and particle motion components, and the relationship between these two depends strongly on the propagation range and environment [4,6,7]. This makes the mechanistic understanding of how external sound fields are coupled into internal particle motions for fish inner ears particularly important when interpreting responses measured in the laboratory or in the field.

Fish hearing is commonly described as sound stimuli reaching the inner ear through direct and indirect pathways [8,9]. All teleosts can detect sound with their otolith end organs through the direct pathway, where the sensory hair cells respond to particle motion through a vibration difference, due to inertial lag because of dense calcareous otoliths responding more slowly to sound stimuli than surrounding soft tissues. Some teleost species can also sense sound through the indirect pathway, where a gas-filled cavity contributes by locally converting acoustic pressure fluctuations into additional motion that can stimulate the inner ear [10–12]. In teleosts with a swim bladder, or other gas-filled chambers, pressure-driven compression and expansion of the gas volume can drive oscillation of the bladder wall and act as a secondary source of particle motion near the sensory epithelia; when anatomical coupling is present (e.g., Weberian ossicles in otophysans), this contribution can be more effective [6,13–15]. These concepts motivate quantitative characterisation of swim bladder resonance properties because they constrain how the bladder responds to pressure excitation and, in turn, what motion this may induce locally [9,16–18]. Accordingly, quantifying swim bladder resonance metrics is a necessary precursor to more ambitious questions, such as how swim bladder resonance varies with fish size and morphology, how it changes with environmental loading (e.g., depth and pressure), and how it may be altered by pathology or damage. These questions are increasingly relevant in freshwater and near-shore settings, where fish behaviour and deterrence are of practical concern (e.g., guiding fish passage at barriers, mitigating entrainment, and reducing ecological impacts of infrastructure).

Despite this motivation, direct measurements of swim bladder resonance properties remain limited. Field-based methods, such as ring hydrophone (i.e., a circular hydrophone geometry used on the cylindrical fish cage to measure the re-radiated sound field from the swim bladder and isolate its resonance signatures in open water) arrangements and related open-water scattering measurements, can resolve the resonance re-radiation, but are logistically demanding and sensitive to boundary effects, such as surface reflections, requiring deep water and careful deployment [19–21]. Laboratory approaches have included ultrasound-based measurements of bladder wall motion (e.g., NIVAMS), but these typically require anaesthesia and precise positioning, and are difficult to reproduce without specialised apparatus [6]. More recent CT-informed modelling has enabled detailed prediction of swim bladder mechanics and pressure sensitivity, but it is not a direct measurement technique and often relies on imaging conditions that are difficult to achieve on unanaesthetised, freely behaving fish [22,23].

In parallel, there has been renewed interest in developing compact, closed experimental systems for measuring resonance of free and/or encapsulated bubbles, motivated

by both fundamental bubble acoustics and applied noise control concepts. Water-filled tubes and small tanks have been used to measure bubble resonance through controlled excitation and pressure recording [24–26], and analogous strategies have been applied to tethered encapsulated bubbles and arrays for underwater noise abatement [27,28]. These studies demonstrate that, with careful experimental design, sub-wavelength gas cavities can be characterised in confined laboratory geometries, but they also highlight an important complication: the resonance of the bubble can couple with, and modify, the host cavity response, so robust identification benefits from an analysis framework that separates the driven system dynamics from the bubble characteristics.

Building on previous laboratory studies that measured free and encapsulated bubble resonance in water-filled tubes and small tanks, a repeatable experimental procedure was developed and reported for identifying the resonance response of an encapsulated gas cavity in a fully water-filled stainless-steel impedance tube, using inflated latex balloons as surrogate swim bladders [29]. That study established the feasibility of detecting and quantifying a cavity resonance peak in this bounded, driven configuration using power spectral analysis, and it clarified practical requirements for repeatability (notably complete water filling and control of unintended air pockets). The present paper advances the same measurement concept from surrogates to biological swim bladders by applying the impedance tube protocol to recently euthanised brown trout (*Salmo trutta*). This intermediate step retains a naturally inflated swim bladder over a short post mortem window while permitting post-test dissection to confirm inflation state and gross morphology, thereby providing a controlled route to evaluate whether the resonance features for the swim bladder, as a damped organ surrounded by soft tissues, remain detectable through this method. To support interpretation under the experimental loading, the measured resonance features are further examined using coupled finite element (FE) modelling.

Swim bladder resonance is often introduced by analogy with the resonance of a free bubble in water, for which the natural frequency decreases with increasing bubble radius and increases with hydrostatic pressure [30,31]. In this framework, the gas acts as a compressible spring, and the surrounding water provides inertia, yielding a sub-wavelength monopole-like response with omnidirectional radiation. In practice, this implies strong near-field pressure gradients and associated particle motion in the vicinity of the oscillating cavity, which are the mechanical quantities most directly relevant to otolithic stimulation and to any bladder-to-ear coupling pathways. For a swim bladder, the same physical picture is useful but incomplete: the gas is bounded by an elastic bladder wall, the cavity is typically elongated and may be chambered, and the surrounding soft tissue introduces additional stiffness and damping. Classical modelling studies therefore treat the swim bladder as an encapsulated gas cavity whose resonance depends on cavity geometry, wall compliance, and environmental loading [16,32–34]. The implication for measurement is that resonance frequency is not determined by size alone, and the quality factor is expected to be substantially lower than for an unbounded bubble, due to viscoelastic and tissue losses.

From a sensory perspective, the relevance of resonance is twofold. First, a resonant gas cavity can amplify local particle motion and pressure gradients in its vicinity, which may be detected directly by otolithic organs. Second, in species with mechanical coupling between the bladder and inner ear, bladder motion can be transmitted efficiently to the sensory epithelia, improving pressure sensitivity and extending the upper frequency limit of hearing [18]. These mechanisms motivate explicit measurement of resonance metrics in laboratory and management contexts, including fishery passages where acoustic deterrence may be deployed. Resonance metrics may also be relevant when selecting exposure frequencies in applied contexts, but the present study reports mechanical characterisation only.

A persistent difficulty is that many environments of interest, like rivers, channels, and shallow reservoirs, do not permit classical far-field measurement paradigms at the frequencies relevant to swim bladder resonance. Limited depth and complex boundaries promote strong multipath effects and reverberation, and the relationship between acoustic pressure and particle motion can vary substantially over short spatial scales. In addition, shallow-water waveguide effects introduce frequency-dependent propagation constraints: for some species and size classes, swim bladder resonance frequencies may fall below the low-frequency cut-off of the environment, so efficient propagation to far-field ranges is not guaranteed even before considering interference and boundary losses. Here, 'low-frequency cut-off' refers to the shallow-water waveguide constraints where, below a certain geometry-dependent frequency, efficient propagation of low-order modes is limited, and the sound fields can become strongly range-limited. These constraints help explain why resonance-specific measurements have historically relied on open-water experiments in deep sea lochs or quarries, where surface reflection artefacts can be controlled and propagation more closely approximates free-field conditions [19,20]. In contrast, compact laboratory methods that resolve resonance properties under controlled conditions can provide a repeatable baseline and enable systematic exploration of factors such as size, shape, inflation state, and wall mechanical properties. The work reported here adopts that approach using a pre-existing stainless-steel, water-filled impedance tube that met the practical requirements for controlled excitation and repeatable hydrophone measurements, allowing method development and validation without the logistical constraints of open-water deployments.

It is also important to clarify the scope of the present study with respect to animal handling. The experiments reported here are not non-invasive: resonance properties are estimated from recently euthanised fish, and the protocol is designed to preserve natural swim bladder inflation for a limited post mortem window while enabling immediate verification by dissection. The value of this intermediate stage is methodological: it tests whether resonance features of a damped biological cavity can be detected reliably in a compact, bounded system, and whether the extracted metrics are sufficiently robust to support interpretation and modelling. These outcomes provide an experimentally grounded foundation for subsequent development of truly non-invasive measurements on live, free-swimming fish in a dedicated test chamber, which is treated separately and will build directly on the procedures and validation reported in this paper.

2. Materials and Methods

2.1. Impedance Tube Configuration

A 1 m long stainless-steel tube (inner diameter 0.10 m, wall thickness 1 cm) was used as a closed, fully water-filled test container. Each end was sealed with a 2 mm thick stainless-steel plate, and the plates were clamped to the tube flange using eight M10 bolts and a 2.5 cm thick removable steel lid [29]. An inertial shaker was mounted to one end plate to inject broadband vibration into the water column. The tube and lid incorporated machined ports to accommodate the shaker and wall-mounted hydrophones, as well as to facilitate filling (Figure 1). Prior to every run, the assembly was filled to eliminate trapped air, because residual pockets can introduce spurious resonances and degrade measurement repeatability.

The experimental configuration is shown in Figure 2. A Data Physics (Riverside, USA) GW-IV45 inertial shaker (mechanical resonance frequency 30 Hz, inertial mass 4.2 kg) was mounted to an end plate providing broadband excitation. A band-limited pseudorandom white noise signal was generated in MATLAB (The MathWorks, Inc., Natick, USA) R2020a and delivered via a National Instruments (Austin, USA) USB-6361 Data Acquisition and a Data Physics PA30E power amplifier (driving voltage 3 V). Two Brüel & Kjær (Virum,

Denmark) 8103 hydrophones (−211 dB re 1 V/µPa), mounted through the tube wall near the upper surface, recorded acoustic pressure signals inside the tube. The hydrophones were positioned at approximately 0.10 m and 0.20 m from the end plate opposite the shaker, providing two pressure channels for consistency checking and for mitigating localised features. Acoustic signals were recorded at a sampling frequency of 4 kHz for a 100 s excitation period.

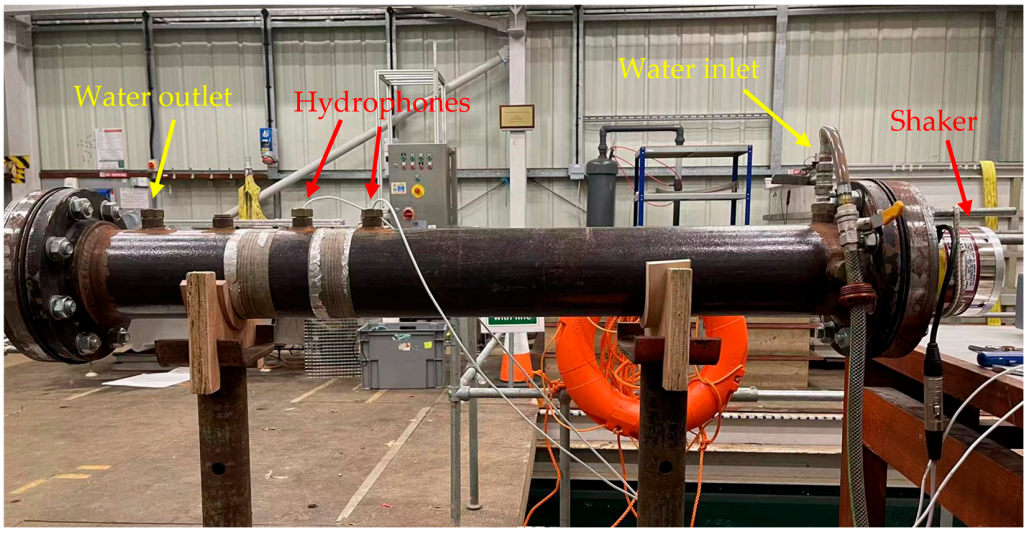

Figure 1. Photo of the pre-existing stainless-steel impedance tube.

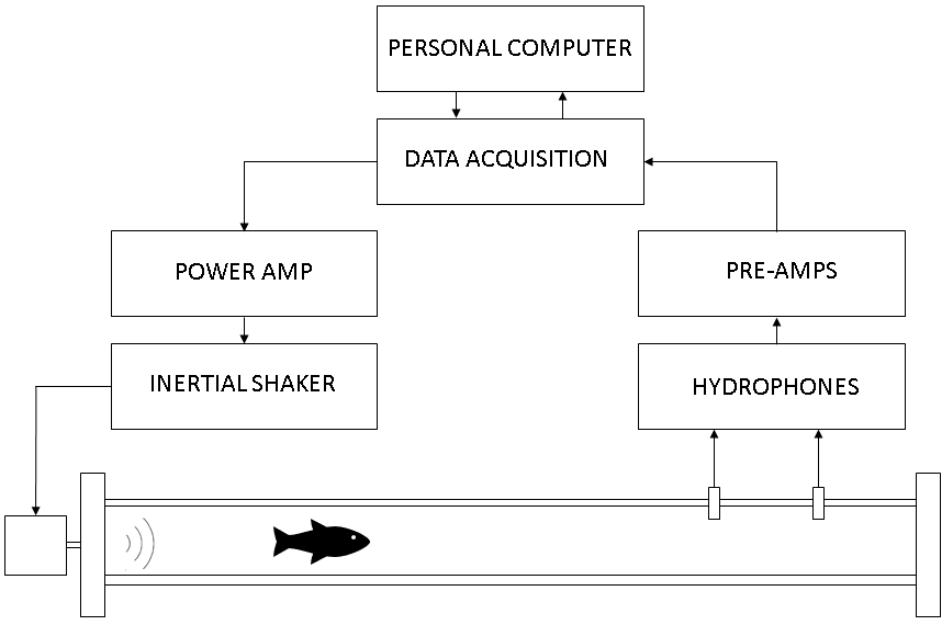

Figure 2. A schematic of the experimental apparatus, approximately to scale. The impedance tube had an internal diameter of 10 cm and a total length of 1 m. The target was placed inside the water-filled tube and was excited by the inertial shaker.

2.2. Targets and Specimen Preparation

Prior work established the impedance tube protocol using inflated latex balloons as surrogate encapsulated gas cavities [29]. The present study focuses on recently euthanised brown trout to evaluate the method on biologically realistic swim bladders while enabling immediate post-test verification of inflation state and geometry. Brown trout specimens (n = 18) were obtained from a separate approved study at the International Centre for Eco-

hydraulics Research (University of Southampton, UK). Fish were euthanised by overdose of 2-phenoxyethanol, followed by destruction of the brain in accordance with Schedule 1 of the Animals (Scientific Procedures) Act 1986, under the approval of the University of Southampton's Animal Welfare and Ethical Review Board (ERGO ID: 87876.A1). Because post mortem changes may lead to swim bladder deflation, measurements were conducted within approximately 30 min of euthanasia. Fork length was measured for each specimen (mean 22.1 ± 2.1 cm; range 11.0–23.9 cm) before being positioned into the impedance tube (Figure 3). Immediately after each measurement, the swim bladder was exposed by dissection and removal of organs obstructing direct vision and measurement to confirm swim bladder intactness and inflation. The semi-major and semi-minor dimensions were measured by a calliper to estimate eccentricity for the prolate ellipsoid approximation (Figure 4).

Figure 3. Measurement of the fork length of a recently euthanised brown trout.

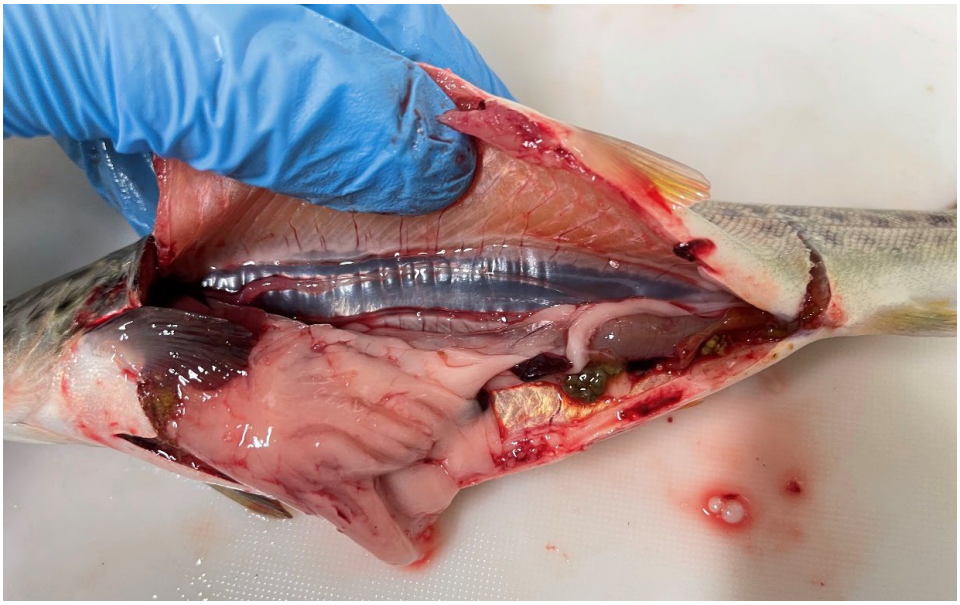

Figure 4. Examination of the intactness of the swim bladder.

2.3. Spectral Estimation and Resonance Properties

For each trial, the system response was characterised in the frequency domain using power spectral density (PSD) and cross-spectral estimates computed from the recorded time series. Spectra were estimated using Welch's method with Hann windowing, 50% overlap, and 1024-sample segments. Welch's method was selected because segment averaging

reduces the variance of the spectral estimator and improves robustness to broadband noise for long, approximately stationary records under pseudorandom excitation. The shaker drive signal, $x(t)$, was saved concurrently with the recorded hydrophone pressure signals, $y(t)$. All channels were sampled synchronously at f_s = 4 kHz for a record duration T = 100 s, providing sufficient averaging to stabilise the spectral estimates in the resonance band of interest.

The time series were partitioned into segments of $N = 1024$ samples (segment duration $N/f_s = 0.256$ s), Hann-windowed, and averaged with 50% overlap. For each channel pair, the one-sided auto-spectral densities, $S_{xx}(f)$ and $S_{yy}(f)$, and the cross-power spectral density, $S_{xy}(f)$, were computed from the discrete Fourier transforms of the windowed segments, and then averaged over all segments. The hydrophone pressure PSD, $S_{yy}(f)$, was used as the primary representation of the system frequency response in this paper because it provides a direct and reproducible depiction of the frequency content of the measured acoustic field under a standardised drive condition. Cross-spectral quantities were used to support quality control, rather than for reporting; specifically, $S_{xy}(f)$ and the magnitude-squared coherence, $\gamma^2(f) = |\, S_{xy}(f)\,|^2 \,/\big(S_{xx}(f)S_{yy}(f)\big)$, were inspected to confirm that spectral features in the resonance band were causally associated with the applied excitation, rather than incidental noise or transient handling artefacts.

Before bubble resonance peak extraction, the empty-tube baseline spectrum was acquired repeatedly under the same acquisition settings and used as the steady reference state for that setting. The fish-present spectrum was then compared directly against the baseline to identify inclusion-associated changes. Where two hydrophones were available, spectra were computed independently for each hydrophone. Agreement between channels in peak frequency and peak prominence was used as an internal consistency check that the observed feature reflected a global response of the coupled tube–fish system, rather than a localised pressure anomaly at a single sensor.

To provide a quantitative indicator that the tube filling procedure yielded a consistent 'empty-tube' reference state, the empty-tube baseline spectrum was re-acquired before each specimen measurement. Baseline repeatability was summarised over 200 to 800 Hz by the median absolute difference (in dB) between the current baseline PSD and a reference baseline run under the same acquisition settings. Across trials, the baseline median absolute difference was typically $\leq$1 dB, with no narrowband emergent peaks indicative of unintended trapped air. In addition, when two hydrophones were available, baseline spectra agreed closely in shape over the same band, and fish-present peak frequencies extracted from the two hydrophones were required to agree within $\pm$5 Hz for a trial to be considered internally consistent, otherwise the specimen was repositioned and/or the tube refill procedure repeated.

Resonance frequency, f_0, was defined operationally as the frequency of the dominant swim bladder-related peak in the PSD of the recorded signal that (i) was absent in the empty-tube baseline, (ii) occurred within the expected frequency band for trout swim bladders under the present setting, and (iii) was repeatable across short repeated acquisitions within the same specimen where available. Peak identification was performed on $10\log_{10}$PSD with consistent handling of bandwidth, using a local maximum criterion within a bounded search interval set to exclude prominent fixed cavity peaks that were present in the baseline.

The resonance sharpness was quantified via a quality factor, Q, computed using the conventional -3 dB bandwidth definition, $Q = f_0/\Delta f$, where $\Delta f = f_2 - f_1$ is the full width at half power of the peak (i.e., the frequency interval where the PSD drops to one-half of its peak amplitude, corresponding to -3 dB on a log scale). Because the observed peaks occur in a bounded cavity with nearby cavity-related spectral features (the empty-tube baseline), Q is interpreted here as an operational descriptor of peak breadth under the

present experimental loading, rather than as a direct estimate of a single intrinsic material damping parameter of the swim bladder wall.

To quantify extraction repeatability, f_0 and Q were computed independently for each hydrophone and compared; a trial was considered internally consistent if the two estimates of f_0 agreed within a pre-specified tolerance (e.g., ± 5 Hz), and if the half-power crossings were well defined on both channels. If a peak was clearly present in one channel, but ambiguous in the other due to local interference, the specimen was re-measured after repositioning or refilling checks, and the more consistent acquisition was retained for analysis.

Although the tube is spatially bounded, f_0 was extracted independently from two hydrophones at different axial locations, and agreement between channels was used as an internal consistency check. When the peak was ambiguous in one channel, the specimen was repositioned and the acquisition repeated. These steps were intended to reduce sensitivity to local pressure anomalies and to ensure that the extracted f_0 reflects a consistent coupled response of the container–specimen system.

2.4. Summary of Numerical Modelling Strategy

FE modelling was used to verify the physical interpretation of the measured resonance features and to examine how a gas-filled swim bladder responds under acoustic excitation. All simulations were performed in COMSOL Multiphysics (version 6.1, Stockholm, Sweden) using 3D object interface. The model was formulated as a coupled acoustic–structure interaction problem in the frequency domain, with the surrounding water and the swim bladder gas represented using the Pressure Acoustics, Frequency Domain module, and the swim bladder wall represented as a thin elastic layer using Structural Mechanics (Shell) module. The shell formulation was selected because it allows wall thickness, elastic properties, and damping to be prescribed directly at the fluid–wall boundary and avoids the need to explicitly mesh a very thin solid domain, while still capturing the dominant wall compliance effects relevant to resonance. Acoustic–Mechanic coupling was implemented via Acoustic–Structure Boundary multiphysics coupling, ensuring that acoustic pressure loads drive wall deformation and that wall motion, in turn, modifies the acoustic fields in the adjacent fluid domains.

To approximate free-field excitation for interpreting the natural resonance of an encapsulated gas cavity, the swim bladder was embedded at the centre of a spherical water domain (radius 0.5 m). The excitation was implemented as a monopole source in the water domain positioned 0.20 m below the swim bladder. A harmonic volume flow rate was prescribed for the monopole (0.0001 m^3/s), and frequency domain solutions were computed from 10 Hz to 1000 Hz in 10 Hz increments. The governing acoustic field in the fluid was solved using the inhomogeneous wave equation in the frequency domain following Equation (1) [35,36]:

$$\frac{1}{\rho_0 c_S^2}\frac{\partial^2 p}{\partial t^2} + \nabla \cdot \left(-\frac{1}{\rho}\nabla p\right) = Q_m, \tag{1}$$

where ρ_0 and c_S represent the static density and sound speed of the medium, respectively. p represents the dynamic sound pressure after the source is induced to radiate sounds, and ρ is the resulting variable density in the medium. The initial sound source Q_m is given as a point source in the following form:

$$Q_m = \frac{4\pi}{\rho_0} S\partial(x - x_0), \tag{2}$$

where S has the following form:

$$S = e^{j\phi} \frac{i\omega\rho_0 Q_S}{4\pi}, \tag{3}$$

and Q_S gives the volume flow rate from the source at $x = x_0$, which was set to 0.0001 m^3/s.

To couple the interaction between the fluid and solid media, the pressure continuity condition should satisfy $F_p = -\vec{n} \cdot p$, where F_p is the pressure load on the boundary, p is the pressure, and $\vec{n}$ is the normal vector. To reduce reflections at the model boundary, the exterior field was treated using an outgoing wave (radiation) condition consistent with spherical spreading. In addition, a perfectly matched layer (PML) surrounded the outer edge of the water domain so that outward-propagating waves were absorbed, approximating an unbounded medium.

The swim bladder was represented as an air-filled prolate ellipsoid to capture the first-order effect of elongation while retaining a tractable parameterisation. The semi-major and semi-minor axes were set from post-test measurements (example parameter set: $a_a = 5.4$ cm, $a_b = 0.7$ cm; eccentricity $\epsilon = a_b/a_a = 0.124$), which correspond to an equivalent spherical radius $r_{\mathrm{eq}} = 1.34$ cm for volume-matched comparison. Water was assigned density 1000 kg/m^3 and sound speed 1480 m/s; the gas domain was assigned density 1.204 kg/m^3 and sound speed 343 m/s. The swim bladder wall was modelled as a linear elastic shell with density 1050 kg/m^3, Young's modulus 2 MPa, and Poisson's ratio 0.45, consistent with recent modelling studies [23]. Wall thickness was set to 0.1 mm, and structural losses were represented using an isotropic loss factor (structural damping) of 0.18. These parameters were not tuned to fit individual measurements; rather, they were chosen to be biologically plausible and sufficient to test whether the observed peak frequencies and peak breadths were consistent with a compliant walled gas cavity.

The model was discretised using a free tetrahedral mesh with physics-controlled refinement. Mesh density was chosen so that element size in the acoustic domains was well below the shortest wavelength over the frequency range of interest. Convergence was verified by checking stability of the predicted resonance peak location under mesh refinement. Model outputs were extracted at the scanning frequencies as sound pressure and the wall displacement at the swim bladder wall to confirm that the dominant spectral feature corresponded to a bladder wall oscillation mode. Results from the FE model were used to support attribution of the experimentally observed peaks to simulated swim bladder resonance and to provide qualitative guidance on the influence of wall compliance and loading assumptions under the present experimental conditions.

The FE model in this study is a free-field verification model, intended to test whether the observed dominant spectral peak is consistent with a compliant walled gas cavity resonance, and to inspect the associated bladder wall motion and local acoustic field. It does not include the impedance tube geometry, end-plate forcing, hydrophone ports, or specimen–wall proximity conditions. Consequently, the model is not used to predict spatial pressure distributions in the empty tube or in the tube with fish present, nor to reproduce tube mode shapes; those container-specific fields would require a dedicated tube geometry in acoustic–structure coupling model and are reserved for future work.

3. Results

3.1. PSDs of the Empty Tube and Tube with Fish Present

Figure 5 overlays representative PSD estimates measured in the fully water-filled impedance tube under driven broadband excitation, comparing the empty-tube baseline (blue) with the response obtained after introducing a recently euthanised brown trout (orange). The empty-tube spectrum provides a practical reference for the intrinsic response of the bounded system, exhibiting repeatable spectral features associated with the tube

geometry, plate bending modes, and compliant boundaries. In our measurements, these baseline features were stable, provided the tube was refilled consistently and unintended trapped air was avoided [29].

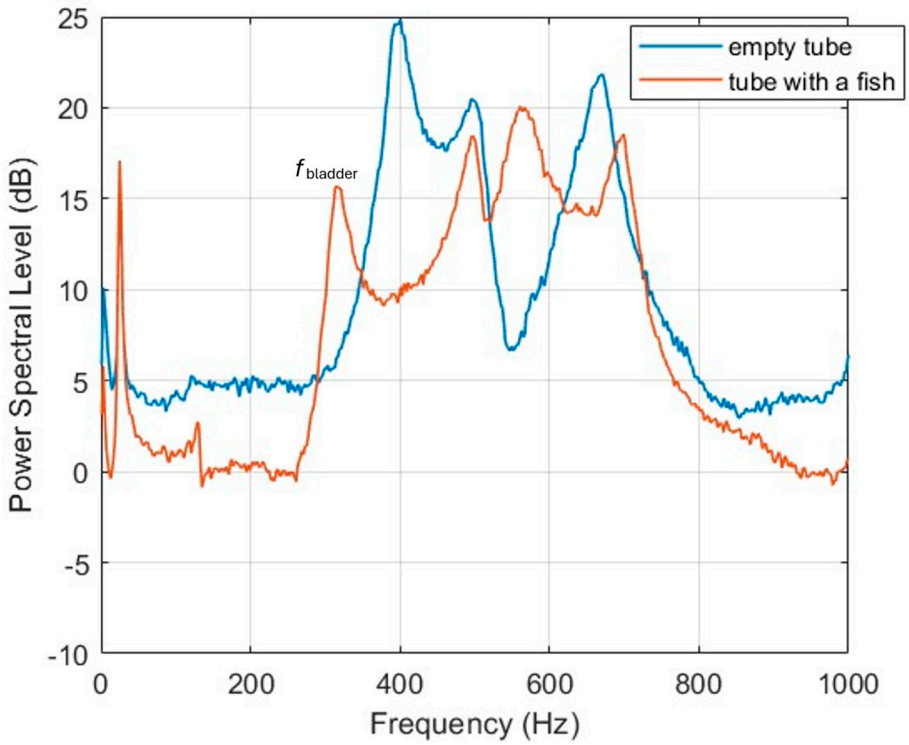

Figure 5. PSD estimates of signals recorded in the impedance tube filled with only water (blue), and water with a 22.3 cm recently euthanised fish inside the tube (orange).

With the fish present, the PSD departs from the empty-tube baseline in two ways (Figure 5). First, a prominent additional peak appears at 316 Hz that is absent in the empty-tube response. This feature is the candidate swim bladder-related resonance used to extract resonance frequency f_0 and the -3 dB bandwidth for an operational quality factor Q. Second, the broader spectral shape is modified: several baseline features, like the three peaks of the empty tube at around 400 Hz, 490 Hz, and 660 Hz, are attenuated and shifted to higher frequencies. These coupled changes are consistent with the introduction of a compliant, gas-filled inclusion that interacts with the tube's bounded response, rather than with incidental electrical noise or differences in the excitation [19,27,29]. All PSDs shown were computed using identical spectral estimation settings and excitation conditions to ensure that differences primarily reflected the presence of the specimen, rather than processing choices.

3.2. Resonance Frequency and Damping as a Function of Body Length

Across the 18 brown trout, the swim bladder resonance frequency extracted from the hydrophone PSD decreased with increasing body length (Figure 6). This trend is consistent with the expectation that larger fish tend to possess larger gas volumes and, therefore, lower characteristic resonance frequencies, when all else is equal. The inverse-length scaling originally proposed from open-water measurements on marine species was given by $f_0 = 7232/L$, where f_0 is in Hz and L is fish length in cm [19]. In the present freshwater trout dataset, this saltwater-based scaling systematically overestimated the measured resonance frequencies. A pragmatic modification that improves agreement for these measurements is $f_0 = 5983/L$, which is used here as a predictor for freshwater fish under the present conditions (black solid line in Figure 6). One plausible anatomical

basis for this offset is that freshwater physostomes commonly carry a larger swim bladder volume fraction (8% of body volume) than many marine species (5% of body volume), which would tend to reduce f_0 [34]. The modified constant is an empirical adjustment based on the Minnaert equation [30] to determine the resonance frequency for a spherical air bubble, calculated (using the physical parameters of an air bubble in water just below the ocean surface) from the difference between swim bladder volume fractions, rather than species-specific morphology, bladder shape, and wall properties, which can all shift resonance relative to a simple length-based predictor. In addition, the slightly higher density of seawater would, all else equal, reduce resonance frequency by roughly 1.2% relative to freshwater, according to Minnaert equation, which is a small effect compared with other biological and morphological factors, but included here for completeness [30].

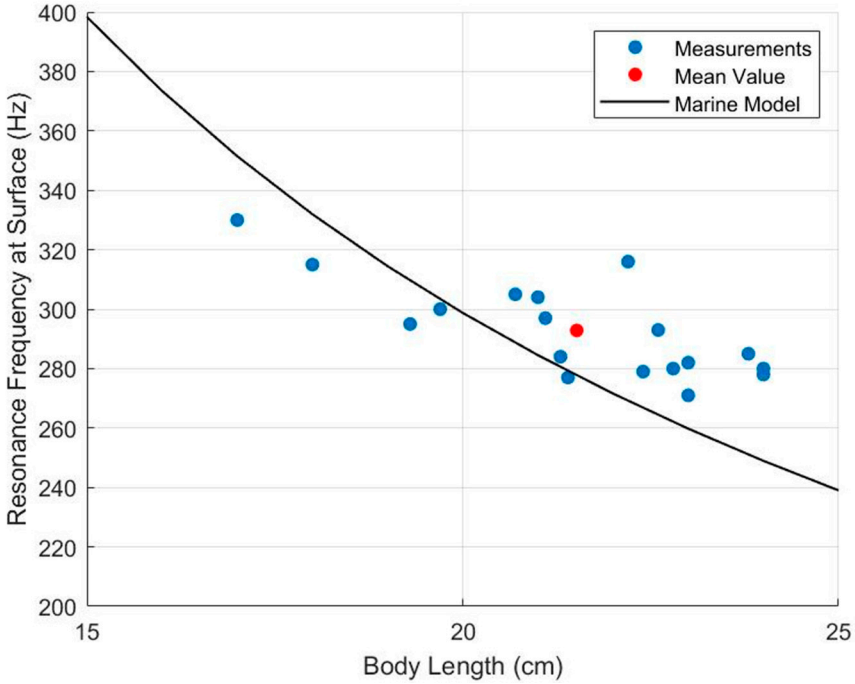

Figure 6. Measured swim bladder resonance frequency vs. fish body length of euthanised brown trout; the solid black curve represents the modified marine model for freshwater fish.

In contrast to resonance frequency, the quality factor showed no clear dependence on body length over the measured range (Figure 7). Within this dataset, the absence of a clear Q-length trend is consistent with earlier direct measurements reporting that damping in swim bladder-bearing fishes is governed primarily by biological loading and loss mechanisms (e.g., tissue viscoelasticity, coupling constraints, and boundary/contact conditions), rather than by gross body size alone [6,21]. Furthermore, the quality factor reported here should not be interpreted as an intrinsic material property of the swim bladder wall. Because the resonance is extracted from the pressure response of a bounded, mechanically coupled system, the measured Q reflects system-level damping of the coupled tube–water–fish–swim bladder configuration, including contributions from surrounding tissues, constraints/contact within the container, and the local acoustic field structure. It is therefore most appropriate for internal comparisons within the same apparatus and protocol (e.g., between specimens, inflation states, or controlled loading conditions), while its direct translation to free-swimming or open-water conditions is limited.

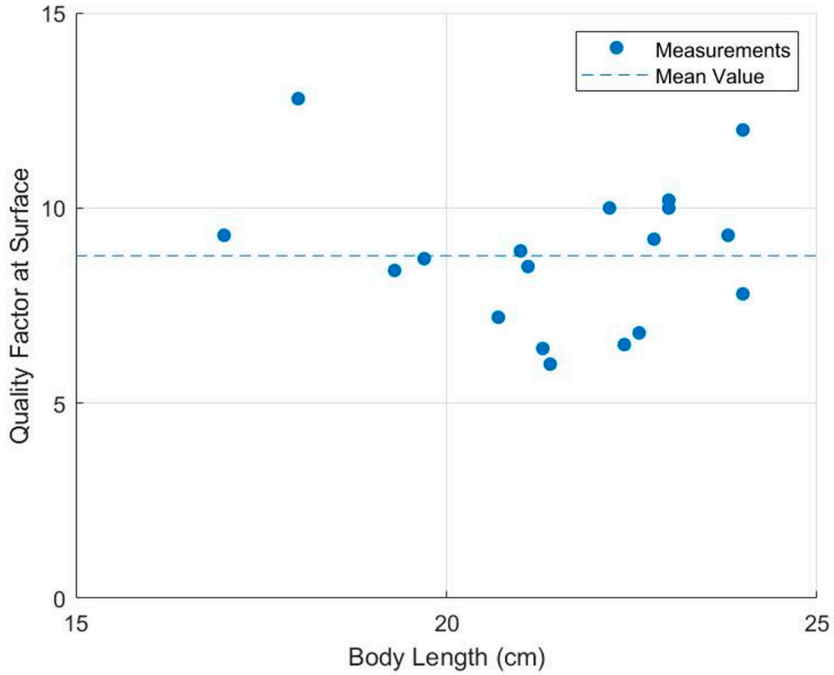

Figure 7. Measured quality factor vs. fish body length of euthanised brown trout; the dashed line represents the mean value of measured quality factors of fish swim bladders.

Finally, it is worth noting that damping may differ between physiological states. The measurements here were made on recently euthanised fish, where muscle tone and tissue mechanical properties may not match those of live, freely behaving individuals. Likewise, pathological changes that modify swim bladder wall stiffness, thickness, or gas volume are expected to alter both f_0 and Q. These considerations do not affect the primary observation that f_0 varies systematically with body length in this dataset, but they motivate future work comparing resonance metrics between live and euthanised conditions, and across health states, using the same experimental framework.

3.3. Numerical Simulations and Comparison with Fish-Present Measurements

Using a geometry and parameter set corresponding to the representative specimen described before, the simulated response exhibited a clear resonance feature at 310 Hz. This simulated resonance lies close to the measured peak at 316 Hz for the same specimen (Figure 8), with the remaining difference smaller than the 10 Hz frequency increment used in the frequency sweep. The model therefore reproduces the observed resonance band without any specimen-specific parameter tuning beyond setting a plausible ellipsoidal geometry and wall properties, supporting attribution of the measured peak to swim bladder resonance under the experimental loading.

Beyond peak location, the simulations were used to examine whether the peak breadth was broadly compatible with the measured damping. The simulated resonance was less damped than the measurement, with a higher operational quality factor (approximately $Q \approx 15$ in the representative simulation vs. $Q \approx 9.7$ for the measured specimen in Figure 4). This difference is consistent with the modelling simplifications: the FE representation includes wall losses via an imposed structural loss factor, but it does not explicitly represent additional dissipation and constraint from surrounding soft tissues, skeletal structures, and contact conditions within the tube, all of which can broaden the measured peak and reduce the apparent Q. Exploratory sensitivity checks (varying wall loss factor and effective thickness) confirm that added losses broaden the peak as expected, but quantitative tissue-layer modelling is underconstrained without independent tissue property measurements.

In this sense, the FE results provide a conservative check that the measurements indicate that biological loading is likely to be a significant contributor to the observed damping in the euthanised specimens. A dedicated extension incorporating a viscoelastic tissue layer or impedance boundary condition that can better represent the surrounding soft tissue is identified as future work.

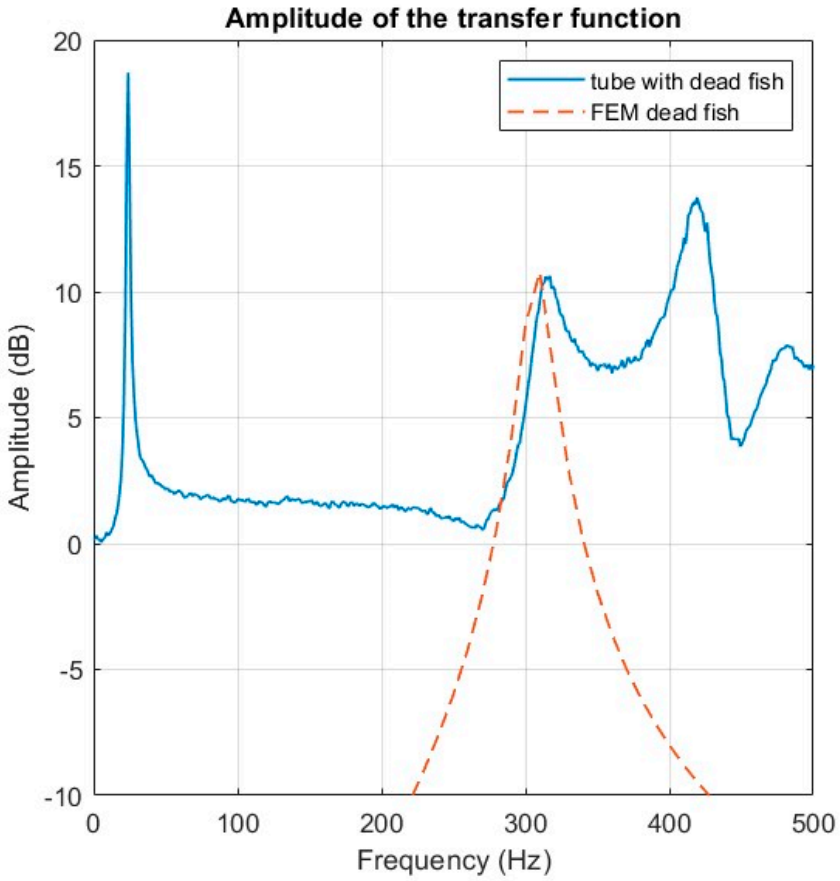

Figure 8. Transfer functions of the measured frequency response of the tube with a fish (blue solid line) and the simulated frequency response of the swim bladder (dashed orange line).

To provide qualitative confirmation that the dominant spectral feature corresponds to a resonance of the swim bladder, rather than a numerical artefact, the simulated fields were inspected across frequency. Near the simulated resonance, the swim bladder wall response and the surrounding acoustic field were consistent with a predominantly volumetric oscillation of the encapsulated gas cavity (Figure 9). At frequencies off resonance, the surface pressure patterns on the ellipsoid became more spatially structured, with volume coupling, once wall motion became increasingly out of phase with the driving sound pressure component, resulting in a reduced surface sound pressure level. These field characteristics are used here only as diagnostic evidence that the model's dominant peak reflects physically interpretable inclusion dynamics.

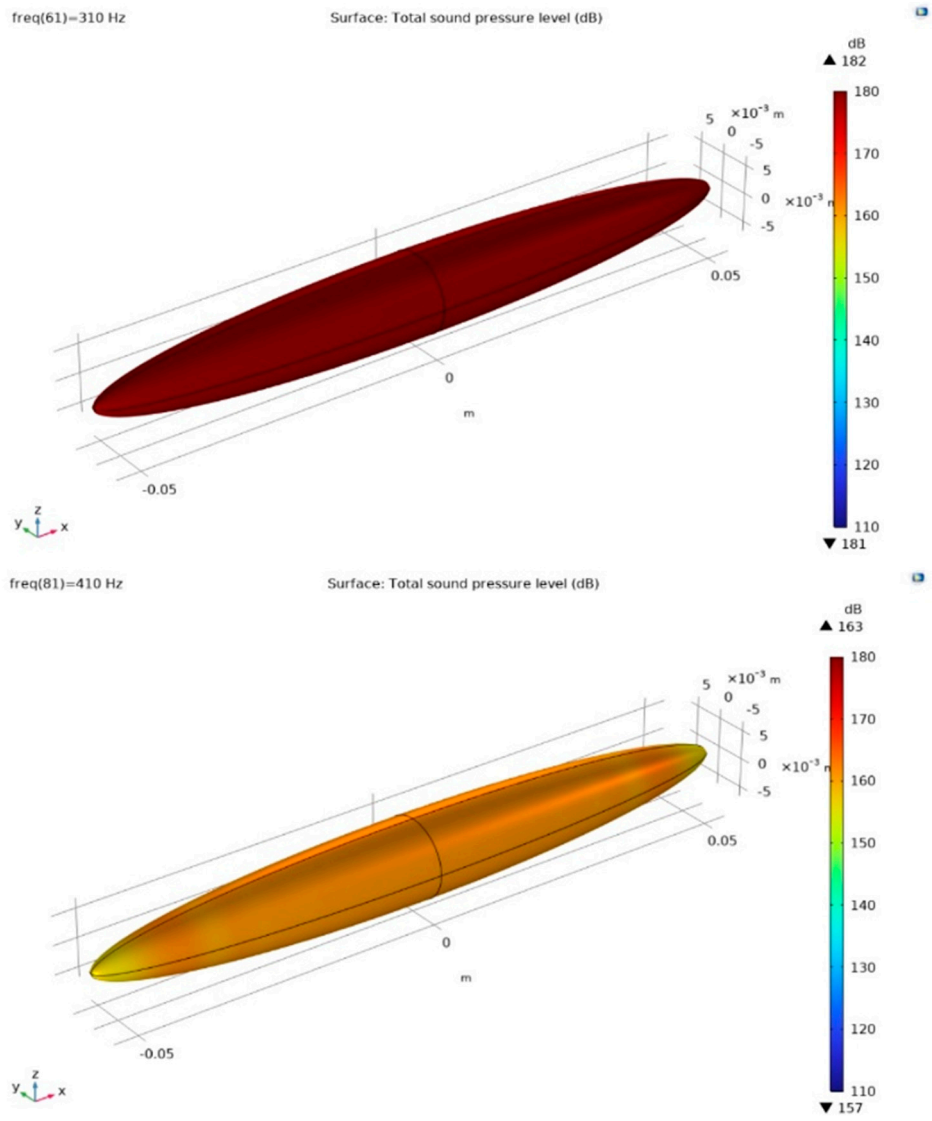

Figure 9. Comparison of simulated sound pressure levels of the modelled swim bladder at the test frequency of 310 Hz (resonance frequency with uniform pressure distribution) and at 410 Hz, which presented a special surface pressure distribution pattern, with the tips of the modelled swim bladder showing lower sound pressure.

4. Discussion

4.1. Bubble Elongation and Minnaert Resonance Frequency

For the representative 22.3 cm trout, the resonance frequency predicted by the Minnaert equation using the equivalent spherical radius of the swim bladder ($a_{\mathrm{eq}} = 1.34$ cm) was 258.5 Hz [30]. This provides a useful baseline, but is expected to underestimate resonance because teleost swim bladders are typically elongated, rather than spherical. For an elongated air bubble, the resonance frequency can be approximated by the following equation [6,33]:

$$f_{elongated} = \frac{x(\varepsilon)}{2\pi a_{equivalent}} \sqrt{\frac{3\gamma_{eff} p_0}{\rho_w}} = x(\varepsilon) f_0, \quad (4)$$

where a_{eq} is the equivalent equilibrium spherical bubble radius, $x(\varepsilon)$ is a correction factor accounting for elongation, and $\varepsilon = a_b / a_a$ is the eccentricity parameter defined by the minor and major semi-axes of the prolate ellipsoid. This formulation carries the same idealisations as Minnaert's result for an unbounded gas bubble in water and neglects bladder wall

tension, as well as γ_{eff}, the frequency-dependent effective polytropic exponent associated with cyclic compression and rarefaction of the gas. For typical swim bladder sizes, however, gas compression is expected to be close to adiabatic, except for a thin thermal boundary layer; therefore $\gamma_{\text{eff}} \approx \gamma \approx 1.4$ was adopted. Here, $\gamma = 1.4$ is the adiabatic index of air; adiabatic compression is a reasonable approximation at these frequencies and cavity sizes because thermal diffusion over one acoustic cycle is confined to a thin boundary layer. The elongation correction factor can be computed as follows [33]:

$$x(\varepsilon) = \varepsilon^{-1/3}\left(1-\varepsilon^2\right)^{1/4}\log^{-1/2}\left(\frac{1+\sqrt{1-\varepsilon^2}}{\varepsilon}\right). \quad (5)$$

which predicts that elongation increases the resonance frequency relative to an equivalent spherical bubble. Using $a_{\text{eq}} = 1.34$ cm and $\varepsilon = 0.124$ for the 22.3 cm trout, Equations (4) and (5) give an estimated resonance frequency of 302.3 Hz for the elongated bubble model. This estimate is closer to the observed resonance peak at 316 Hz in the impedance tube measurements, supporting the interpretation that the elongation of the bubble is a primary contributor to the upward shift from the simple Minnaert prediction.

The remaining difference between the elongated bubble estimate (302.3 Hz) and the measured resonance frequency (316 Hz) is consistent with additional stiffening and loading mechanisms not included in Equations (4) and (5). In particular, the swim bladder is an encapsulated gas cavity embedded in surrounding soft tissues (Figure 4), so wall and tissue constraints can introduce an effective surface tension-like restoring contribution that increases the resonance frequency further [31]. This is consistent with the experimental finding that the measured resonance frequency was higher than the elongated bubble estimate, while the resonance peak was also more damped (lower Q factor) than would be expected for an idealised gas bubble, reflecting additional dissipation mechanisms associated with the bladder wall and surrounding biological structures.

Moreover, because hydrostatic pressure also strongly affects gas cavity resonance, atmospheric pressure measurements here provide a surface baseline only. Even shallow depths can shift f_0 appreciably under bubble-like scaling, motivating future pressure-controlled measurements and/or modelling-based pressure compensation as a necessary step toward field deployment.

4.2. Frequency Shift and Attenuation of Tube Modes Due to Bubble Resonance

Figure 5 shows that introducing a fish into the impedance tube not only adds a distinct low-frequency resonance peak (attributed to the swim bladder), but also modifies the pre-existing tube spectral features: several baseline peaks are attenuated, and their centre frequencies shift. By definition, such changes cannot occur without an inclusion; the empty-tube response is the reference system. The consistent frequency shift and amplitude decrease in tube-related features that happened in all measurements, therefore, points to a coupled system effect: the resonant gas inclusion modifies the effective dynamics of the host cavity, rather than simply superimposing an additional isolated resonance peak.

A physically plausible explanation for this behaviour is available from the theory of linear wave propagation in bubbly liquids [37]. In the Commander–Prosperetti (CP) model, a bubble–liquid mixture is treated as an effective medium whose macroscopic acoustic properties (phase speed and attenuation) depend on the physical properties and relative fractions of the constituent phases [27,38,39]. Although the CP model is formally derived for a population of bubbles (a bubbly liquid), it was applied to the single-bubble case by representing the system in terms of an effective void fraction and a representative bubble size [27]. It is to be noted that this is a qualitative, heuristic application: CP theory is derived for a spatially distributed bubble population, whereas the present system

contains a single and non-spherical inclusion. Here, it is used only to provide a physically plausible mechanism for the observed direction of system mode shifts and attenuation, consistent with prior encapsulated bubble tank studies using an effective void fraction approximation [27,28]. Following their approach, the same framework is used here to interpret how a single encapsulated gas cavity, such as latex balloon or swim bladder, perturbs the impedance tube resonances. The key parameter is the void fraction β, defined as the ratio of gas volume V_g to the total mixture volume V_m,

$$\beta = \frac{V_g}{V_m}. \tag{6}$$

In the CP formulation, the bubble population is characterised by a size distribution $n(a)$ over bubble radius a. For a monodisperse distribution (all bubbles the same size), this simplifies to the following:

$$n(a) = N\,\delta(a - a_0), \tag{7}$$

where N is the number density and $\delta(\cdot)$ is the Dirac delta function [27]. Under this description, the CP model predicts a complex phase speed $c_m(\omega)$ for the effective medium [37],

$$\frac{1}{{c_m}^2} = \frac{1}{{c_0}^2} + 4\pi \int_0^\infty \frac{a\wp(a)da}{{\omega_{CP}}^2 - \omega^2 + 2ib\omega}, \tag{8}$$

with the bubble resonance frequency, ω_{CP}, and damping terms governing dispersion and losses:

$$\omega_{CP} = 2\pi f_{CP}, \tag{9}$$

$$f_{CP} = f_0 - \frac{1}{2\pi a}\sqrt{\frac{2\sigma}{\rho_w a}} = \frac{1}{2\pi a}\sqrt{\frac{3\gamma P_{b0}}{\rho_w} - \frac{2\sigma}{\rho_w a}}, \tag{10}$$

where f_0 is the Minnaert frequency; the additional term $-2\sigma/\rho_w a$ accounts for liquid surface tension σ, which is absent in Minnaert's model. Acoustic energy dissipation is described by the damping term:

$$b(\omega, a) = \frac{2\mu}{\rho_w a^2} + \frac{P_{b0}}{2\rho_w a^2 \omega}\mathrm{Im}\phi + \frac{\omega a^2}{2c_w}, \tag{11}$$

which describes losses due to viscous, thermal, and acoustic re-radiation processes, respectively, and the term ϕ was previously given by Equation (3) [37].

A central qualitative prediction of CP theory is that the effective phase speed and attenuation become strongly frequency-dependent in the vicinity of the bubble resonance. For frequencies below the bubble resonance, bubble wall motion is in phase with the driving pressure, the mixture is acoustically soft, and the phase speed is reduced relative to bubble-free water. Above resonance, bubble wall motion becomes out of phase, the effective stiffness increases, and the phase speed can rise sharply; a corresponding attenuation peak occurs near resonance due to energy dissipation mechanisms (thermal, viscous, and acoustic re-radiation), with re-radiation expected to dominate for the large bubble sizes relevant to encapsulated balloons and swim bladders [37]. This behaviour is illustrated in the CP predictions for a monodisperse distribution, where phase speed increases rapidly above resonance, and attenuation remains elevated over a band above resonance [27]. The introduction of an encapsulated bubble shifted a tank resonance upward (from 320 Hz to approximately 355 Hz) while reducing peak amplitude, consistent with dispersion and attenuation in the effective medium induced by bubble resonance [27]. Later, an encapsulated bubble array produced systematic upward shifts across multiple tank modes and reduced amplitudes for modes above the bubble resonance, consistent with bubble-

induced attenuation above f_0 [38,39]. These experiments motivate the hypothesis that a single encapsulated bubble or swim bladder in the impedance tube can similarly modify the tube mode structure through effective medium behaviour, even though the mixture is spatially localised in reality.

Applying the same effective void fraction logic to the present tube, the swim bladder volume can be represented by an equivalent spherical radius $a_{mean} = a_{\mathrm{eq}} = 1.27$ cm. With $V_{\mathrm{bladder}} = 8.7$ mL and tube water volume $V_{\mathrm{tube}} = 6170.7$ mL, the implied void fraction is $\beta \approx 0.14\%$. Using CP predictions for this β and a, the phase speed around the shifted tube mode band is increased relative to bubble-free water (Figure 10). In the same analysis, the original first tube resonance (397 Hz, assuming $c = 1480$ m/s) corresponds to a wavelength $\lambda_{\mathrm{tube}} = 3.78$ m. After introducing the swim bladder, the first tube resonance shifts to 497 Hz; the CP-predicted phase speed near 500 Hz was $c_m \approx 1991$ m/s, giving $\lambda_{CP} \approx 3.98$ m, i.e., a modest increase (5.2%) in the effective wavelength compared with the empty-tube condition. Consistent with the sensitivity check, allowing the dynamic viscosity of surrounding tissue to vary from 50 to 80 produces phase speed predictions spanning the observed shifted resonance range, with the measured 497 Hz lying within that range [33]. While this calculation is not a strict inversion (CP assumptions are idealised, and the tube field is not a plane wave in an infinite medium), it provides a plausible mechanistic interpretation: above the swim bladder resonance, the local effective stiffness increases, and elevated attenuation predicted by CP theory can shift tube modes upward and reduce their amplitudes.

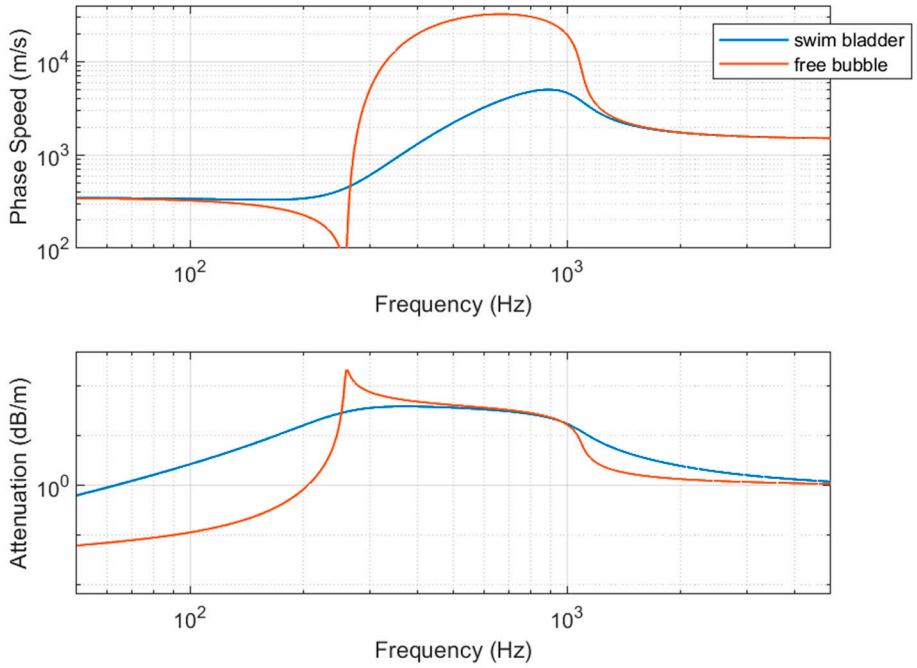

Figure 10. Predicted sound speed and attenuation from CP model with the swim bladder (blue) vs. a free bubble (orange) in the impedance tube with a = 1.27 cm and β = 0.14%.

4.3. Relevance of Measured Swim Bladder Resonance to Fish Hearing and Behaviour

The resonance frequency and quality factor estimated in this study are mechanical descriptors that characterise how efficiently acoustic pressure can induce oscillatory motion of the swim bladder and its surrounding tissue. These parameters are central to the indirect pressure-to-motion pathway in teleost auditory processing, where a gas-filled cavity, such as the swim bladder, acts as a mediator by converting pressure fluctuations into mechanical displacements in the near field. This displacement may then be transduced by inner ear

sensory structures, particularly in species with anatomical coupling (e.g., Weberian ossicles), but potentially also in non-specialists through general body cavity mechanics [6,13,14].

Because the present measurements are based on pressure spectra in the bounded container, and do not directly quantify particle motion (particularly at the inner ear), hearing-related implications are restricted to mechanistic context; no hearing thresholds or behavioural outcomes are inferred from these data. Rather, the findings demonstrate that the swim bladder resonance band is mechanically measurable under laboratory conditions, and that this band varies systematically with body size (Figure 6), which also suggests that FE-based numerical modelling method can estimate the swim bladder resonance frequencies, while the damping mechanism is complicated to model [22,23,40]. This method provides a physically grounded starting point for designing future auditory or behavioural studies. For instance, if fish are exposed to tonal stimuli in a behavioural assay, the observed relationship between resonance frequency and body length can inform the selection of stimulus frequencies, specifically in choosing conditions at, below, and above the resonance band, instead of relying on arbitrary or fixed-frequency protocols.

It is important to recognise that the resonance values measured in this study are derived under specific experimental conditions: post mortem, bounded within an impedance tube, and at atmospheric pressure. These settings yield repeatable and well-characterised results suitable for validation against numerical models, but they do not reflect the full complexity of in vivo or in situ environments. For example, hydrostatic pressure (i.e., water depth) alters the swim bladder's internal pressure and mechanical stiffness, shifting resonance frequency upward while potentially reducing effective damping [17,31,40,41]. Similarly, the loss of muscle tone post mortem may reduce mechanical tension on the bladder wall, influencing compliance and introducing differences from live physiology. Although measurements were performed within 30 min of euthanasia to preserve swim bladder inflation, post mortem loss of muscle tone and time-dependent changes in tissue viscoelasticity can modify constraint and dissipation pathways around the swim bladder. These changes are expected to affect peak breadth (operational Q) more strongly than peak frequency, through increased soft-tissue shear losses and altered contact conditions. This provides a plausible contribution to the lower measured Q compared with the simplified FE model, which does not explicitly represent surrounding tissues or contact constraints.

In the present setup, the operational quality factor provides a compact descriptor of the resonance bandwidth of the coupled fish–tube system, via $\Delta f \approx f_0/Q$ using the -3 dB definition. For the representative case ($f_0 \approx 316$ Hz, $Q \approx 9.7$), this corresponds to a half-power bandwidth of order $\Delta f \approx 33$ Hz, indicating that the mechanically inferred pressure-to-bladder-motion response is not confined to a single narrow frequency bin, but extends over a finite band around f_0 under the present loading. Mechanistically, this suggests that, if a fixed tonal stimulus is selected close to the expected resonance band for a given size class, modest detuning from f_0 (e.g., due to inter-individual size variation in f_0 within that class) would be expected to reduce the peak mechanical response progressively, rather than eliminate it abruptly. However, the present measurements quantify system-level mechanical bandwidth in a post mortem, bounded configuration; whether and how such bandwidth translates to effective bandwidth in vivo, or to any behavioural responses, cannot be inferred from these data and require dedicated validation.

Therefore, the present study aims at establishing a validated experimental and modelling framework that enables subsequent investigations under more biologically realistic conditions. By linking experimental resonance estimates to FE predictions and morphological measurements, the work supports the hypothesis that resonance-mediated amplification may contribute to sound detection or discrimination (i.e., enhanced bladder wall motion and associated near-field particle motion/pressure gradients in the surrounding tissues

near resonance, which can increase mechanical stimulation at the otolith organs and/or via bladder–ear coupling) [42]. Whether such mechanisms play consistent or functionally significant roles across species, contexts, or behavioural states remains a topic for targeted empirical investigation.

5. Conclusions

This study demonstrates that swim bladder resonance properties in recently euthanised brown trout can be identified reproducibly in a compact, fully water-filled impedance tube using PSD-based analysis under controlled broadband excitation. Relative to the empty-tube baseline, fish-present measurements consistently show an additional dominant peak attributable to a resonant gas-filled inclusion and systematic modification of surrounding tube spectral features, consistent with coupled cavity-inclusion dynamics.

Across 18 specimens, the extracted resonance frequency decreases with body length and is reasonably described by an inverse-length relationship, while the operational quality factor shows no clear size dependence over the measured range. These trends support the interpretation that fish size primarily controls the gas volume which sets f_0, whereas damping is governed more by tissue losses and experimental loading.

Coupled acoustic–structure FE simulations reproduce the principal resonance band and peak character for a representative specimen and provide mechanistic support for attributing the measured peak to swim bladder resonance. The remaining differences in peak breadth are consistent with additional biological and contact-related damping mechanisms not explicitly represented in the simplified ellipsoidal model.

The present study establishes a repeatable laboratory protocol for resonance identification under controlled boundary and filling conditions. The current stainless-steel tube system is a laboratory prototype and is not intended as a field-deployable instrument in its present form. However, the approach could, in principle, be translated to a portable closed-container implementation, provided that future engineering development addresses practical requirements including reliable filling, robust sealing, repeatable transducer mounting, stable excitation and power, and mitigation of ambient vibration and acoustic interference in real sites. Such a portable implementation could support non-invasive comparative measurements of resonance properties across individuals or timepoints, for example, in studies assessing whether swim bladder condition (including potential pathological states) is associated with measurable changes in the resonance band.

Overall, the results provide a calibrated methodological basis and an interpretation framework for subsequent studies that aim to refine modelling with specimen-specific geometry and more efficient experimental protocol, as well as connect resonance-informed mechanical properties to hearing-relevant hypotheses and behavioural responses under laboratory and, ultimately, field-relevant conditions.

Author Contributions: Conceptualisation, W.L.W., P.K. and P.R.W.; methodology, P.R.W. and W.L.W.; software, W.L.W.; validation, W.L.W. and P.R.W.; formal analysis, W.L.W.; investigation, W.L.W. and P.E.; resources, P.K.; data curation, W.L.W.; writing—original draft preparation, W.L.W.; writing—review and editing, W.L.W.; visualisation, W.L.W.; supervision, P.R.W. and P.K.; project administration, W.L.W.; funding acquisition, P.K. All authors have read and agreed to the published version of the manuscript.

Funding: This research was funded by European Union Horizon 2020 Research and Innovation Programme under the Marie Sklodowska-Curie Actions, Grant Agreement No. 860800.

Institutional Review Board Statement: The animal study protocol was approved by the Animal Welfare and Ethical Review Board of the University of Southampton (ERGO ID: 87876.A1; Approval date: 26 October 2023).

Data Availability Statement: The data that support the findings of this study are available from the corresponding author upon reasonable request.

Acknowledgments: We thank J Cheer for the equipment and Y Cai for project assistance.

Conflicts of Interest: The authors declare no conflicts of interest.

Abbreviations

The following abbreviations are used in this manuscript:

PML	Perfectly Matched Layer
FE	Finite Element
PSD	Power Spectral Density
CP	Commander–Prosperetti

References

1. Krause, B.B. Anatomy of the soundscape evolving perspectives. *J. Audio Eng. Soc.* **2008**, *56*, 73–80.
2. Mann, D.A.; Lobel, P.S. Propagation of damselfish (*Pomacentridae*) courtship sounds. *J. Acoust. Soc. Am.* **1997**, *101*, 3783–3791. [CrossRef]
3. Hawkins, A.D.; Amorim, M.C.P. Spawning sounds of the male haddock, Melanogrammus aeglefinus. *Environ. Biol. Fishes* **2000**, *59*, 29–41. [CrossRef]
4. Montgomery, J.; Jeffs, A.; Simpson, S.; Meekan, M.; Tindle, C. Sound as an orientation clue for the pelagic larvae of reef fish and crustaceans. *Adv. Mar. Biol.* **2006**, *51*, 143–196.
5. Sueur, J.; Farina, A. Ecoacoustics: The Ecological Investigation and Interpretation of Environmental Sound. *Biosemiotics* **2015**, *8*, 493–502. [CrossRef]
6. Cox, M.; Rogers, P.H. Automated noninvasive motion measurement of auditory organs in fish using ultrasound. *J. Vib. Acoust.* **1987**, *109*, 55–59. [CrossRef]
7. Thode, A.M.; Sakai, T.; Michalec, J.; Rankin, S.; Soldevilla, M.S.; Martin, B.; Kim, K.H. Displaying bioacoustic directional information from sonobuoys using "azigrams". *J. Acoust. Soc. Am.* **2019**, *146*, 95–102. [CrossRef]
8. Sisneros, J.A.; Rogers, P.H. Directional hearing and sound source localization in fishes. In Fish hearing and bioacoustics: An anthology in honor of Arthur N. Popper Richard R. Fay. *Adv. Exp. Med. Biol.* **2016**, *877*, 121–155.
9. Vetter, B.J.; Sisneros, J.A. Swim bladder enhances lagenar sensitivity to sound pressure and higher frequencies in female plainfin midshipman (*Porichthys notatus*). *J. Exp. Biol.* **2020**, *223*, jeb225177. [CrossRef]
10. Popper, A.N.; Fay, R.R. Sound Detection and Processing by Fish: Critical Review and Major Research Questions (Part 2 of 2). *Brain Behav. Evol.* **1993**, *41*, 26–38. [CrossRef]
11. Hudspeth, A.J. The Cellular Basis of Hearing: The Biophysics of Hair Cells. *Science* **1985**, *230*, 745–752. [CrossRef] [PubMed]
12. Schulz-Mirbach, T.; Ladich, F.; Plath, M.; Heß, M. Enigmatic ear stones: What we know about the functional role and evolution of fish otoliths. The role of fish otoliths in inner ear function. *Biol. Rev.* **2018**, *94*, 457–482. [CrossRef]
13. Popper, A.N.; Fewtrell, J.; Smith, M.E.; McCauley, R.D. Anthropogenic Sound: Effects on the Behavior and Physiology of Fishes. *Mar. Technol. Soc. J.* **2003**, *37*, 35–40. [CrossRef]
14. Popper, A.N.; Fay, R.R. Rethinking sound detection by fishes. *Hear. Res.* **2011**, *273*, 25–36. [CrossRef]
15. Ladich, F. Peripheral hearing structures in fishes: Diversity and sensitivity of catfishes and cichlids. In Fish Hearing and Bioacoustics: An Anthology in Honor of Arthur N. Popper Richard R. Fay. *Adv. Exp. Med. Biol.* **2016**, *877*, 321–340.
16. Love, R.H. Resonant acoustic scattering by swimbladder-bearing fish. *J. Acoust. Soc. Am.* **1978**, *64*, 571–580. [CrossRef]
17. Feuillade, C.; Nero, R.W. A viscous-elastic swimbladder model for describing enhanced-frequency resonance scattering from fish. *J. Acoust. Soc. Am.* **1998**, *103*, 3245–3255. [CrossRef]
18. Popper, A.N.; Hawkins, A.D. An overview of fish bioacoustics and the impacts of anthropogenic sounds on fishes. *J. Fish Biol.* **2019**, *94*, 692–713. [CrossRef]
19. McCartney, B.; Stubbs, A. Measurements of the acoustic target strengths of fish in dorsal aspect, including swimbladder resonance. *J. Sound Vib.* **1971**, *15*, 397–420. [CrossRef]
20. Sand, O.; Hawkins, A.D. Acoustic properties of the cod swimbladder. *J. Exp. Biol.* **1973**, *58*, 797–820. [CrossRef]
21. Lo/Vik, A.; Hovem, J.M. An experimental investigation of swimbladder resonance in fishes. *J. Acoust. Soc. Am.* **1979**, *66*, 850–854. [CrossRef]
22. Salas, A.K.; Wilson, P.S.; Fuiman, L.A. Ontogenetic change in predicted acoustic pressure sensitivity in larval red drum (*Sciaenops ocellatus*). *J. Exp. Biol.* **2019**, *222*, jeb201962. [CrossRef]

23. Li, H.; Gao, Z.; Song, Z.; Su, Y.; Hui, J.; Ou, W.; Zhang, J.; Zhang, Y. Investigation on the contribution of swim bladder to hearing in crucian carp (*Carassius carassius*). *J. Acoust. Soc. Am.* **2024**, *155*, 2492–2502. [CrossRef]
24. Leighton, T.G.; White, P.R.; Morfey, C.L.; Clarke, J.W.L.; Heald, G.J.; Dumbrell, H.A.; Holland, K.R. The effect of reverberation on the damping of bubbles. *J. Acoust. Soc. Am.* **2002**, *112*, 1366–1376. [CrossRef]
25. Wilson, P.S.; Roy, R.A.; Carey, W.M. An improved water-filled impedance tube. *J. Acoust. Soc. Am.* **2003**, *113*, 3245–3252. [CrossRef]
26. Argo, T.F.; Wilson, P.S.; Palan, V. Measurement of the resonance frequency of single bubbles using a laser Doppler vibrometer. *J. Acoust. Soc. Am.* **2008**, *123*, EL121–EL125. [CrossRef] [PubMed]
27. Lee, K.M.; McNeese, A.R.; Tseng, L.M.; Wochner, M.S.; Wilson, P.S. Measurements of resonance frequencies and damping of large encapsulated bubbles in a closed, water-filled tank. *Proc. Meet. Acoust.* **2012**, *18*, 075003. [CrossRef]
28. Lee, K.M.; Wilson, P.S.; Wochner, M.S. Attenuation of standing waves in a large water tank using arrays of large tethered encapsulated bubbles. *J. Acoust. Soc. Am.* **2014**, *135*, 1700–1708. [CrossRef] [PubMed]
29. Wu, L.; White, P.R.; Kemp, P. Measurements of the Resonance Properties of Dummy Fish Swim Bladders. In *International School of Hydraulics*; Springer Nature: Cham, Switzerland, 2023; pp. 397–407.
30. Minnaert, M. On musical air-bubbles and the sounds of running water. *Philos. Mag.* **1933**, *16*, 235–248. [CrossRef]
31. Leighton, T. *The Acoustic Bubble*; Academic Press: Cambridge, MA, USA, 1994.
32. Andreeva, I. Scattering of sound by air bladders of fish in deep sound-scattering ocean layers. *Sov. Phys. Acoust.* **1974**, *10*, 17–20.
33. Weston, D.E. Sound propagation in the presence of bladder fish. In *Underwater Acoustics*; Albers, V.M., Ed.; Plenum Press: New York, NY, USA, 1967; Volume 2, pp. 55–88.
34. Bone, Q.; Moore, R. *Biology of Fishes*; Taylor & Francis: Oxford, UK, 2008.
35. Kinsler, P.; Kelsall, R.W.; Harrison, P. Interface and confined phonons in stepped quantum wells. *Phys. B Condens. Matter* **1999**, *263*, 507–509. [CrossRef]
36. Bruneau, M. *Fundamentals of Acoustics*; Wiley: New York, NY, USA, 2013.
37. Commander, K.W.; Prosperetti, A. Linear pressure waves in bubbly liquids: Comparison between theory and experiments. *J. Acoust. Soc. Am.* **1989**, *85*, 732–746. [CrossRef]
38. Lee, K.M.; Hinojosa, K.T.; Wochner, M.S.; Argo, T.F.; Wilson, P.S.; Mercier, R.S. Sound propagation in water containing large tethered spherical encapsulated gas bubbles with resonance frequencies in the 50 Hz to 100 Hz range. *J. Acoust. Soc. Am.* **2011**, *130*, 3325–3332. [CrossRef]
39. Lee, K.M.; Wilson, P.S.; Wochner, M.S. Attenuation of low-frequency underwater sound using an array of air-filled balloons and comparison to effective medium theory. *J. Acoust. Soc. Am.* **2017**, *142*, 3443–3449. [CrossRef] [PubMed]
40. Wu, L. Non-Invasive Method of Measuring Resonance Properties of Fish Swim Bladders. Doctoral Dissertation, University of Southampton, Southampton, UK, 2025.
41. Khodabandeloo, B.; Agersted, M.D.; Klevjer, T.; Macaulay, G.J.; Melle, W. Estimating target strength and physical characteristics of gas-bearing mesopelagic fish from wideband in situ echoes using a viscous-elastic scattering model. *J. Acoust. Soc. Am.* **2021**, *149*, 673–691. [CrossRef]
42. Maiditsch, I.P.; Ladich, F.; Heß, M.; Schlepütz, C.M.; Schulz-Mirbach, T. Revealing sound-induced motion patterns in fish hearing structures in 4D: A standing wave tube-like setup designed for high-resolution time-resolved tomography. *J. Exp. Biol.* **2022**, *225*, jeb243614. [CrossRef] [PubMed]